Magneto-optical studies of excitons in $Zn_{1-x}Cd_xSe/ZnSe$ quantum wells

J. Puls, V. V. Rossin,* and F. Henneberger
Humboldt-Universität zu Berlin, Institut für Physik, 10115 Berlin, Germany

R. Zimmermann
Max-Planck-Arbeitsgruppe ''Halbleitertheorie,'' 10117 Berlin, Germany

(Received 11 December 1995)

Magnetoabsorption on high-quality $Zn_xCd_{1-x}Se/ZnSe$ multiple quantum wells grown by molecular-beam epitaxy is used to study systematically the major excitonic properties. The small inhomogeneous width of the exciton lines allows us to observe Landau levels arising from higher heavy-hole exciton transitions as well as to analyze in detail the spin splitting and diamagnetic shift of the ground state. The Schrödinger equation of magnetoexcitons is solved numerically to describe their magnetic-field behavior and to deduce the relevant excitonic and band parameters in dependence on the Cd content in the well. Anticrossing features at higher Landau levels and the magnetic-field dependence of the light-hole exciton ground-state energy signify a complex valence-band structure due to heavy-light hole coupling. [S0163-1829(96)04031-3]

I. INTRODUCTION

Since the successful *p*-type doping, wide-gap II-VI semiconductor related quantum structures have been promising candidates for commercial laser diodes and related optoelectronic devices operating in the blue spectral range.[1] The absorption edge of bulk II-VI's is dominated by excitons. In quasi-two-dimensional structures, the Coulomb interaction is further enhanced so that excitons may play an important part in the lasing process, even at room temperature.[2] Up to now, a number of studies for $Zn_xCd_{1-x}Se/ZnSe$ multiple quantum wells (MQW's) have been reported[3–8] where the excitonic properties are deduced from a fit of the heavy-hole (hh) and light-hole (lh) exciton ground-state energies. Such fits are based on a detailed knowledge of the composition- and strain-induced band offsets as well as the carrier mass dependent confinement energies of electrons and holes. As known from GaAs-related MQW's, magneto-optics is a more powerful tool for studying both exciton binding energies and band parameters in the two-dimensional case (see, e.g., Refs. 9 and 10). First magneto-optical studies of excitons in ZnSe-related MQW's (Ref. 11) were restricted to the 1*s* and 2*s* hh exciton states from which lower and upper limits of the binding energy were derived. In a previous communication,[12] we have demonstrated the formation of magneto-oscillations in the hh subband absorption of similar MQW's, which enabled us to observe simultaneously the diamagnetic shift of the hh exciton ground state and the conversion of *s*-like excited exciton states into Landau levels.

Here, we present a systematic study of magnetoexcitons in $Zn_{1-x}Cd_xSe/ZnSe$ MQW's with well widths close to the bulk exciton Bohr radius and Cd contents ranging from 7% to 20%. Detailed information about the energetic structure and relevant band parameters is obtained by comparing the experimental data with the results of a numerical solution of the Schrödinger equation for the in-plane motion of the magnetoexcitons.[13] Complementary, we perform a variational treatment of the exciton ground state at zero magnetic field using a two-parameter trial function. The large splitting between the hh and lh exciton in $Zn_xCd_{1-x}Se/ZnSe$ QW's due to the combined action of quantum confinement and compressive in-plane strain justifies one to carry out both calculations in a two-band model. The effects of hh-lh coupling are qualitatively discussed. The excitonic parameters deduced reveal an increase of the exciton binding energy due to quantum confinement and, surprisingly, also of the reduced in-plane exciton mass with growing Cd content. This paper is organized as follows: in Sec. II the numerical solution and variational treatment, respectively, of the Schrödinger equation for the exciton are outlined. In Sec. III we describe the samples, the experimental details, and the results of magnetoabsorption measurements. The analysis of experimental data is performed in Sec. IV and our conclusions are drawn in Sec. V.

II. MAGNETOEXCITONS

In relation with experimental studies on GaAs-related QW's, the theory of magnetoexcitons is well developed.[10,13,14] Here, we summarize the general aspects and the specific approach used for the analysis of our experimental data. A single quantum well of width d_w is considered. The z axis is along the growth direction and $\mathbf{r}_{e,h}=(\boldsymbol{\rho}_{e,h},z_{e,h})$ are the electron and hole coordinates, respectively. Because of the large hh-lh splitting enhanced by the compressive in-plane strain, we restrict our considerations of the hh magnetoexciton first to simple parabolic bands.[15] With the magnetic field perpendicular to the QW plane (Faraday configuration), the vector potentials $\mathbf{A}_{e,h}$ can be chosen in such a way that they contain only in-plane coordinates. We use in the following the symmetrical gauge $\mathbf{A}_{e,h}=(\mathbf{B}\times\boldsymbol{\rho}_{e,h})/2$. Then the motion of carriers can be expressed separately for the in-plane ($\|$) and z direction ($\perp$) and the Hamiltonian of the system reads

$$H=E_g+\sum_{i=e,h}\frac{(\mathbf{p}_{i,\|}-q_i\mathbf{A}_i)^2}{2m_{i,\|}(z_i)}+\sum_{i=e,h}\left(-\frac{\hbar^2}{2}\frac{\partial}{\partial z_i}\frac{1}{m_{i,\perp}(z_i)}\frac{\partial}{\partial z_i}+V_i^*(z_i)\right)-\frac{e^2}{\varepsilon_0|\mathbf{r}_e-\mathbf{r}_h|}, \tag{1}$$

with $q_e=-|e|$, $q_h=|e|$, and the in-plane momentum operator $\mathbf{p}_{e,h,\|}$ of the electron and hole, respectively. The z dependence of the confinement potential $V_i^*(z_i)=V_i\Theta(|z_i|-d_w/2)$ is expressed by the Heaviside step function. E_g is the band gap of the well material and $V_{e,h}$ is the band offset for the electron and the heavy hole, respectively. In (1), the anisotropy of the hole mass and the discontinuity of both carrier masses are explicitly taken into account. Image charges[16] due to different static dielectric constants ε_0 in the well and barrier as well as polaron effects[17] are beyond the scope of this paper because the required material parameters are not precisely enough known for zinc-blende $Zn_xCd_{1-x}Se$ mixed crystals. The in-plane hh mass as well as the hh and lh masses along the z axis follow from the Luttinger parameters by $m_{\mathrm{hh},\|}=m_0/(\gamma_1+\gamma_2)$, $m_{\mathrm{hh},\perp}=m_0/(\gamma_1-2\gamma_2)$, and $m_{\mathrm{lh},\perp}=m_0/(\gamma_1+2\gamma_2)$, respectively. To solve (1) numerically, we use the separation ansatz

$$\psi(\boldsymbol{\rho}_e,\boldsymbol{\rho}_h,z_e,z_h)=\phi(\boldsymbol{\rho}_e,\boldsymbol{\rho}_h)\varphi_e(z_e)\varphi_h(z_h), \tag{2}$$

where subband coupling is neglected. The wave functions $\varphi_{e,h}(z_{e,h})$ are the solutions of the one-particle equations along the z axis using the continuity of φ and $(1/m_\perp)(\partial\varphi/\partial z)$ at the well boundaries. The corresponding confinement energy of the electron and heavy hole are denoted by $E_{\mathrm{qc},e}$ and $E_{\mathrm{qc},h}$, respectively. Since we are interested in direct optical transitions, we omit the center-of-mass momentum. Introducing the relative coordinate $(\boldsymbol{\rho}=\boldsymbol{\rho}_e-\boldsymbol{\rho}_h)$ and the conjugate momentum $\mathbf{p}$, we get by a canonical transformation[18]

$$H'=E_g^*+\frac{p^2}{2\mu_\|}+\frac{e^2}{8\mu_\|}(\mathbf{B}\times\boldsymbol{\rho})^2+\frac{eB}{2\mu_\|}\beta(\boldsymbol{\rho}\times\mathbf{p})+V(\rho) \tag{3}$$

with the effective potential

$$V(\rho)=\int\int dz_e\,dz_h\varphi_e^2(z_e)\varphi_h^2(z_h)\frac{e^2}{\varepsilon_0|\mathbf{r}_e-\mathbf{r}_h|}. \tag{4}$$

$E_g^*=E_g+E_{\mathrm{qc},e}+E_{\mathrm{qc},h}$ is the energy gap between the lowest subbands. Similar to (4), the inverse reduced in-plane mass $1/\mu_\|=1/m_e+1/m_{\mathrm{hh},\|}$ and the ratio $\beta=(m_{\mathrm{hh},\|}-m_e)/(m_{\mathrm{hh},\|}+m_e)$ are integrals over the subband wave functions too. The fourth term on the right-hand side of (3) contains the angular momentum operator $\mathbf{L}=\boldsymbol{\rho}\times\mathbf{p}$ of the internal exciton motion and is, therefore, purely additive. It describes the Zeeman effect and vanishes for s-like exciton states seen in one-photon transitions. Separating the angular motion, we arrive at a one-dimensional Schrödinger equation, which is solved by the finite difference method.[19] Further, we will refer to this treatment by NSIM (numerical solution of in-plane motion).

The separation (2) neglects any electron-hole correlation along the z axis. Whereas such a treatment is justified for excited exciton states with Bohr radii clearly larger than the well width, it might fail for the ground state. We have thus performed a complementary variational treatment of (1) for zero magnetic field using a separation ansatz with a two-parameter exciton envelope function

$$\psi(\rho,z_e,z_h)=\exp\left[-\frac{1}{a}\sqrt{\rho^2+\gamma^2(z_e-z_h)^2}\right]\varphi_e(z_e)\varphi_h(z_h). \tag{5}$$

The parameter a is the Bohr radius and γ accounts for the dimensionality of the exciton. Both parameters are fixed by minimizing the expectation value of (1) treating mass anisotropy and discontinuity in the same way as for the direct numerical solution of (4). The diamagnetic shift of the hh exciton ground state can be calculated within the first-order perturbation theory by[20]

$$\Delta E_{\mathrm{dia}}=\frac{e^2B^2}{8\mu_\|}\langle\rho^2\rangle, \tag{6}$$

where the expectation value of the squared in-plane radius $\langle\rho^2\rangle$ has to be computed from the wave function (5).

The internal motion of the exciton at zero field is usually described by the main quantum number $n=1,2,\ldots$ and $|l|=0,1,\ldots,n-1$ specifying the angular momentum in the z direction. As seen from (3), both remain good quantum numbers in a magnetic field. When the Coulomb term in (3) is ignored, simply the Landau energies

$$E=E_g^*+(n_e+\tfrac{1}{2})\hbar\omega_e+(n_h+\tfrac{1}{2})\hbar\omega_h,\quad n_{e,h}=0,1,2,\ldots \tag{7}$$

are obtained. $\omega_{e,h}=eB/m_{e,h}$ is the cyclotron frequency of the electron and hole, respectively. Although n_e and n_h are not good quantum numbers due to the Coulomb interaction, a magnetic field can be defined for each exciton state above which a Landau-like behavior dominates its magnetic field dependence.[21] In this field range, we refer to them as Landau levels throughout this work, keeping in mind that they are still modified by Coulomb interaction. In the strict two-dimensional case, that modification is given by a $\sqrt{B}$ term.[21]

III. EXPERIMENT

The three samples used in the present study are grown on GaAs(001) substrates by molecular-beam epitaxy (MBE) using a 0.7-μm ZnSe buffer layer. A phase-locked epitaxy mode[22] is used to improve lattice plane completion during growth. The MQW's consist of five wells of width between 4.5 and 5.0 nm. The barrier width is 85 nm to guarantee isolated wells. The ratio between barrier and well widths suggests that the wells adopt the ZnSe in-plane lattice constant and are thus pseudomorphically strained. The Cd content of the well (x_{Cd}) is determined by x-ray and microprobe analysis of thick alloy layers grown with the same molecular beam fluxes. After removing the substrate by a selective wet etching technique, the samples are mounted on a glass substrate. Distinct exciton features are observed in the transmission spectra up to room temperature with an alloy related full width at half maximum of a few meV at 1.8 K. The magneto-optical properties are investigated by conventional transmission experiments using an OXFORD split-coil magnet making available fields up to $B=12$ T. The spectral resolution used in the experiments is better than 0.1 meV. The use of circularly polarized light in Faraday configuration en-

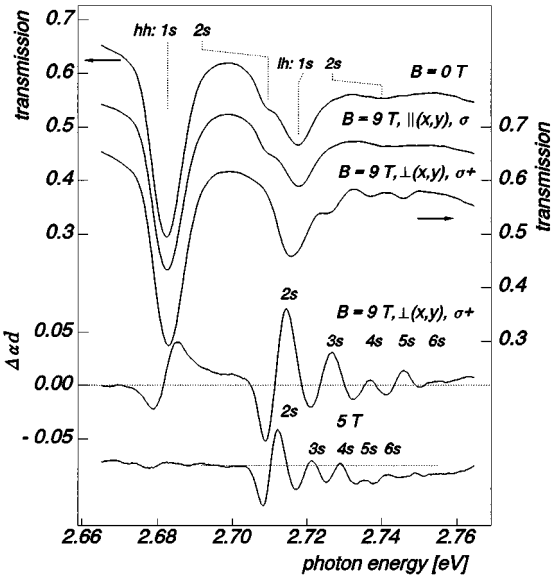

FIG. 1. Transmission spectra of a $Zn_xCd_{1-x}Se/ZnSe$ MQW without and with magnetic field applied parallel (Voigt geometry) and perpendicular (Faraday geometry) to the quantum well plane (x,y), respectively. $d_w=5$ nm. Lower part: Magnetic-field-induced changes of the optical density in Faraday configuration.

ables us to uncover even the very small spin splitting of the various exciton states.

Representative for the samples investigated, the upper curve in Fig. 1 displays the transmission spectrum of the MQW sample with nominal $x_{Cd}=0.13$ in the spectral range from the $1s$ hh exciton ($X_{hh,1s}$) to the continuum states of the lh exciton. The structures of the $2s$ hh exciton ($X_{hh,2s}$) and the lh exciton ground state ($X_{lh,1s}$) are clearly resolved too. Applying a magnetic field of $B=9$ T perpendicular to the QW plane (Faraday configuration), a small high-energy shift of $X_{hh,1s}$ (0.55 meV) is found. For the σ^+ polarization drawn in the lowest transmission curve, both the Zeeman and diamagnetic effect of the exciton ground state contribute to this shift in the same direction. Distinct magneto-oscillations due to the formation of Landau levels are found in the region of the hh subband absorption. The field-induced change of the optical density $\Delta\alpha d$ plotted in the lower part of Fig. 1 shows well-resolved features up to the Landau level arising from the $6s$ exciton state. Except for the $5s$ and $6s$ levels at 9 and 5 T, respectively, a growing damping of the features with increasing photon energy is found. Above 2.76 eV no further levels could be detected. For comparison, the transmission spectrum for a field of $B=9$ T applied parallel to the QW (Voigt configuration) is also drawn in Fig. 1. As expected for the quasi-two-dimensional case, the high-energy shift of $X_{hh,1s}$ is markedly smaller and no magneto-oscillations are observable.

The small inhomogeneous broadening of the exciton lines allows the observation of Landau levels in Faraday configuration already at fields of $B\approx 2$ T. In Figs. 2(a)–2(c), the energy of the hh ground-state exciton and the magnetic-field-induced absorption features are drawn as a function of B for each sample. The data for σ^+ and σ^- polarization are given by pluses and open circles, respectively. The solid lines represent fits of the data with the magnetoexciton calculation discussed in more detail in the next section. The magnetic field behavior of the exciton states is quite different. The ground state exhibits both a diamagnetic shift and a clearly resolved spin splitting (see also Fig. 3). Commonly for all samples, the X_{hh} ground state can be well described by a sum of a zero-field energy, a diamagnetic shift, and a Zeeman splitting:

$$E=E_{hh}+\delta B^2\pm g_{eff}\mu_B B, \tag{8}$$

with the ''+'' sign referring to σ^+ polarization. μ_B is the Bohr magneton. The same Zeeman splitting is found for the excited exciton states with the only exception being the $2s$ state on the $x_{Cd}=0.13$ MQW [Fig. 2(b)]. The reason for its somewhat larger splitting is currently not clear. The higher the excited magnetoexciton state, the closer it follows a linear field dependence. Since the Coulomb correlation is small for these states, they start to behave similarly to uncorrelated

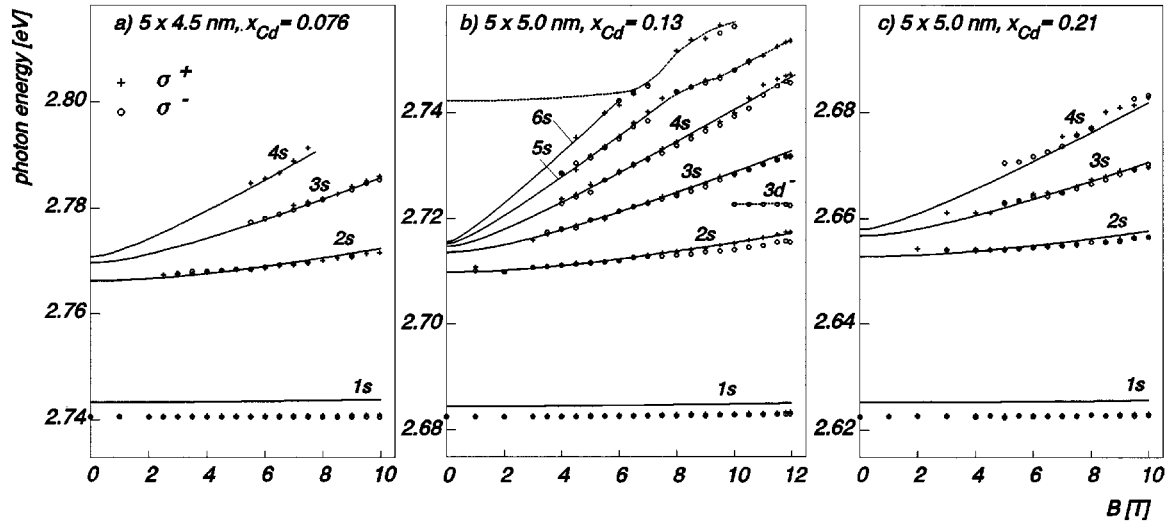

FIG. 2. Energy of exciton absorption peaks vs magnetic field for three different structures. Solid lines: Fit of the data by the calculated magnetoexciton energies. $\varepsilon_0=8.8$ (Ref. 23), $V_e+V_h=(1.35x_{Cd}-0.3x_{Cd}^2)$ eV, $V_e/V_h=0.7/0.3$ (Ref. 8). Dashed lines are used to guide eye.

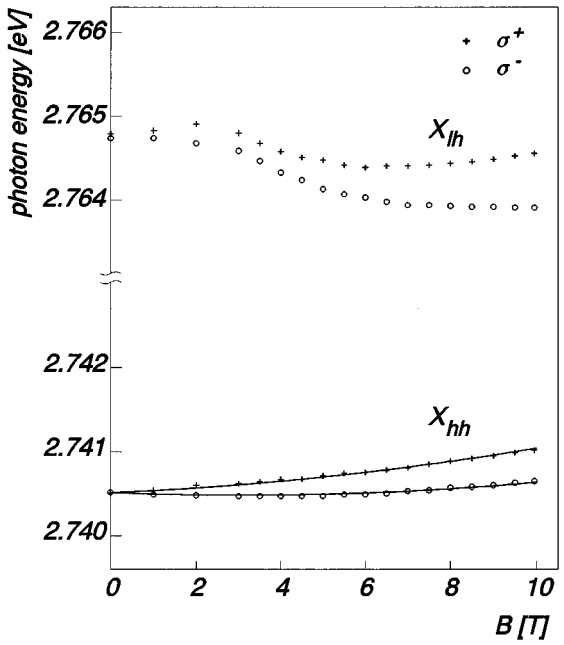

FIG. 3. Magnetic-field behavior of the hh and lh exciton ground state of the MQW with $x_{\mathrm{Cd}}=0.076$ and $d_w=4.5$ nm. Solid lines: fit of the hh exciton ground state by formula (8).

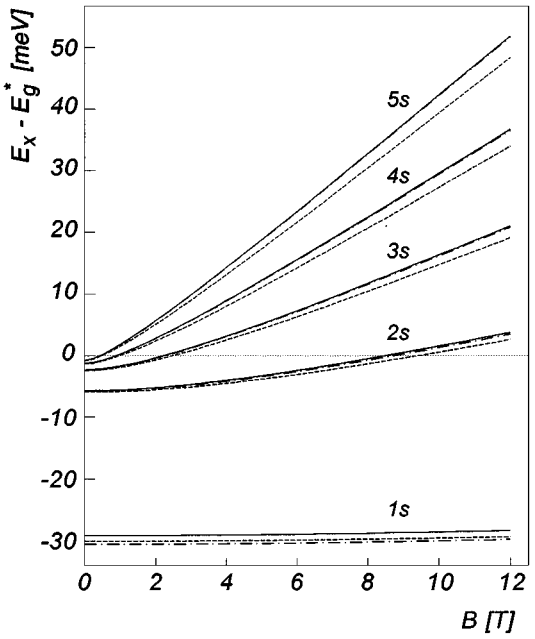

FIG. 4. Calculated magnetoexciton energies measured relatively to E_g^*. $d_w=5$ nm. Solid lines: $V_e=110$ meV; $V_h=47$ meV; $\mu_\parallel=0.099m_0$. Dashed-dotted lines: $V_e=165$ meV; $V_h=71$ meV; $\mu_\parallel=0.099m_0$. Dashed lines: $V_e=110$ meV; $V_h=47$ meV; $\mu_\parallel=0.105m_0$.

electron-hole pairs at relatively low fields. For the sample with $x_{\mathrm{Cd}}=0.13$ in Fig. 2(b), this behavior can be seen until the excited hh states are merged by B into the subband continuum of the lh exciton above 2.74 eV. Beyond this field, clear indications of an anticrossing behavior are found. Similar features are not observed on the other two samples. For higher Cd content [Fig. 2(c)], neither the somewhat larger inhomogeneous broadening nor the increased lh-hh splitting allows one to trace the Landau levels up to the lh exciton continuum, whereas for $x_{\mathrm{Cd}}=0.076$ in Fig. 2(a) that region is covered by the onset of barrier absorption. For the latter sample, the magnetic field behavior of the hh exciton ground state is depicted again in Fig. 3 using an enlarged energy scale. Additionally, the data for the $1s$ lh exciton are given, which exhibit a more complicated behavior. Superimposed to the splitting between the σ^+ and σ^- component, a nonmonotonous dependence on B is observable.

IV. ANALYSIS OF EXPERIMENTAL DATA

For ZnSe-related MQW's, there are still considerable uncertainties about the correct band offsets and carrier masses. Even for bulk ZnSe, two different sets of electron and hole masses are widely used:

$$m_e=0.160m_0, \quad m_{\mathrm{hh},\perp}=0.495m_0,$$

$$m_{\mathrm{lh},\perp}=0.152m_0 \quad (\gamma_1=4.30, \quad \gamma_2=1.14) \tag{9}$$

and

$$m_e=0.147m_0, \quad m_{\mathrm{hh},\perp}=0.813m_0,$$

$$m_{\mathrm{lh},\perp}=0.272m_0 \quad (\gamma_1=2.45, \quad \gamma_2=0.61) \tag{10}$$

determined by Brillouin scattering of excitonic polaritons[24] and magneto-optical studies of p-like excited exciton states,[25] respectively. For the $Zn_xCd_{1-x}Se$ alloy, a linear interpolation between the binary components is usually made where the masses in cubic CdSe are assumed to be 20–25 % smaller than those for ZnSe.[3] In what follows, we extract the information contained in the magneto-optical data of the previous section by comparing them with numerical calculations of magnetoexciton energies. The various parameters enter with quite different importance. This is demonstrated in Fig. 4, where hh magnetoexciton energies computed by the NSIM are drawn versus magnetic field. The solid lines are obtained using the masses in (10) adapted to $x_{\mathrm{Cd}}=0.12$[3] and a total band offset $V_e+V_h=157$ meV shared by $V_e/V_h=0.7/0.3$ between conduction and hh valence band. An increase of the offset by 50% (dashed-dotted lines) yields a low-energy shift of the exciton ground state due to increased confinement, but practically no resolvable changes for the excited exciton states. The latter applies also when V_e/V_h is increased up to 0.8/0.2 and, as long as $\mu_\parallel$ is kept fixed, for a variation of the heavy-hole and electron masses along the z axis. The reason for this is that the alteration of the subband wave functions by those parameters modifies the effective Coulomb potential $V(\varrho)$ in such a way that excited exciton states with smaller probability density near $\varrho=0$ are less affected than the ground state. On the contrary, as seen from the dashed lines in Fig. 4, a change of the reduced in-plane mass by only 5% causes already a significant variation of the excited magnetoexciton energies. Therefore, despite uncertainties remaining for the band offsets and carrier masses in the z direction, the correct values for E_g^* and $\mu_\parallel$ can be precisely derived from their magnetic-field behavior.[26] As demonstrated by Fig. 2, a very satisfactory fit is indeed achieved for

TABLE I. Parameters of the hh exciton obtained by fitting the excited states with the magnetoexciton calculations and the ground state with (8), respectively.

x_{Cd}	d_w (nm)	E_g^* (eV)	R_{hh} (meV)	$\mu_\parallel^*/m_0$	δ (μeV/T^2)	g_{eff}
0.076	4.5	2.772	31.4	0.114	(3.3)	0.35
0.13	5.0	2.716	33.6	0.115	4.4	0.26
0.21	5.0	2.660	37.3	0.122	3.5	0.21

any of the three MQW structures. The resulting subband gaps and reduced in-plane masses are summarized in Table I. Instead of $\mu_\parallel$ representing an average over the subband wave functions, the mass ($\mu_\parallel^*$) is given, which belongs purely to the strained well material. Unlike a previous analysis based only on exciton ground-state data,[3] the fitting procedure reveals an increase of $\mu_\parallel^*$ with growing Cd content. An extrapolation to ZnSe yields a reduced in-plane mass consistent with set (10) rather than (9). Accordingly, all calculations of the present paper rely on the band masses (10) proportionally increased to obtain the reduced in-plane masses given in Table I. It should be noted that, even for the highest fields, both slope and energy spacing of the excited exciton states (Fig. 2) deviate remarkably from the values expected for pure Landau levels. This indicates the significant role still played by the Coulomb interaction. A quite similar behavior has been very recently reported for magnetoexcitons in $CdTe/Cd_xZn_{1-x}Te$ QW's (Ref. 27) with even less exciton binding energies.

As seen from Fig. 2, the agreement between the experimental data and the NSIM calculations is less perfect for the exciton ground states. Nevertheless, since E_g^* is accurately known from the fit of the excited exciton states, the binding energy $R_{hh}=E_g^*-E_{hh}$ can be easily derived using for E_{hh} the experimental position at $B=0$. In addition to R_{hh}, Table I compiles also the magnetic parameters δ and g_{eff} deduced with the aid of the empirical formula (8). The 2.7–2.9-meV smaller values of the exciton binding energy obtained by the NSIM (see Table II) are caused by the neglect of the Coulomb correlation along the z direction in (2).[28] Indeed, a much better description of the ground state is provided by the variational treatment with the two-parameter wave function (5) previously successfully applied to explain exciton data on $Zn_xCd_{1-x}Se/ZnSe$ MQW's with no magnetic field.[5] The computed exciton binding energies given also in Table II are very close to the semiexperimental data in Table I. We have also enumerated the diamagnetic shift coefficient δ using both the magnetic field dependence of X_{hh} directly calculated by the NSIM as well as the exciton wave function (5) of the variational treatment. As seen in Table II, either method yields practically the same values. This shows that, despite the neglected electron-hole correlation along the z direction, the in-plane motion of the ground-state exciton is described correctly by the NSIM too. For the MQW's with higher Cd concentration, the calculated δ coefficients agree very well with the experimental data. From (6), the expectation value of the squared in-plane radius can be determined. An increase of x_{Cd} from 0.13 to 0.21 decreases $\langle\varrho^2\rangle^{1/2}$ from 4.8 to 4.4 nm, reflecting the stronger two-dimensional confinement for larger barriers. The value of δ found for the sample with $x_{Cd}=0.076$ may be already influenced by the coupling with lh states due to the smaller hh-lh splitting. The dependence of g_{eff} on the Cd content indicates also a small but not negligible coupling for the ground state. The valence-band mixing is more clearly seen from the anticrossing features marked by dashed lines in Fig. 2(b) ($x_{Cd}=0.13$) as well as from the magnetic-field behavior of the lh exciton ground state in Fig. 3 ($x_{Cd}=0.076$). In what follows, we present a qualitative discussion of those effects on the basis of the selection rules for the band mixing.

TABLE II. Comparison of the hh exciton ground-state binding energy and the in-plane size obtained from the numerical solution of (4) and the variational treatment.

Sample		NSIM		Variational treatment	
x_{Cd}	d_w (nm)	R_{hh} (meV)	δ (μeV/T^2)	R_{hh} (meV)	δ (μeV/T^2)
0.076	4.5	28.7	5.14	31.1	4.89
0.13	5.0	31.7	4.40	33.3	4.43
0.21	5.0	34.2	3.62	35.8	3.68

In (1), the kinetic energy terms of the hole have to be replaced by the 4×4 $\mathbf{k}\cdot\mathbf{p}$ Hamiltonian for heavy and light holes with the angular momentum $j_h=3/2$ and its projection $j_{z,h}=\pm3/2$ and $\pm1/2$, respectively.[29] In Ref. 14, numerical calculations of magnetoexcitons have been performed within this framework. The modified Hamiltonian commutes neither with the square nor the projection of the angular momenta $\mathbf{J}_h$ and $\mathbf{L}$ arising from Bloch factors and the internal exciton motion, respectively. Instead, the square and projection of the total angular momentum $\mathbf{F}=\mathbf{L}+\mathbf{J}_h$ are good quantum numbers. Moreover, the parity of the excitonic envelope is conserved. Therefore, exciton states $|n,l,j_{z,h}\rangle$ (Ref. 30) of different l and $j_{z,h}$ have to be properly combined to construct simultaneous eigenstates $|f_{z,h}\rangle$ of the Hamiltonian, $\mathbf{F}^2$, F_z, and the parity operator. For s-like hh exciton states ($l=0$), only mixing with excited d-like ($l=\pm2$) lh states occurs:[14,31]

$$|+3/2\rangle=c_{11}|n_1s,+3/2\rangle+c_{12}|n_2d^+,-1/2\rangle \tag{11}$$

and

$$|-3/2\rangle=c_{21}|n_1s,-3/2\rangle+c_{22}|n_2d^-,+1/2\rangle,\quad n_2\geqslant3, \tag{12}$$

being optically active for σ^+ and σ^- polarization, respectively. Due to the Zeeman term in (3), their magnetic-field shift is different. In a pure Landau level picture, $3d^-$ corresponds to a transition between the zeroth electron and the second hole level, whereas $3d^+$ takes place between the second electron and the zeroth hole level. For the coupling between the $1s$-lh exciton state and d-like hh states a similar consideration shows that the mixing with d^+ and d^- hh states appears also in σ^+ and σ^- polarization, respectively. We note that the coupling of hh and lh states is present already at $B=0$. In a magnetic field, this effect can be enhanced by tuning the various states energetically closer or even into resonance.

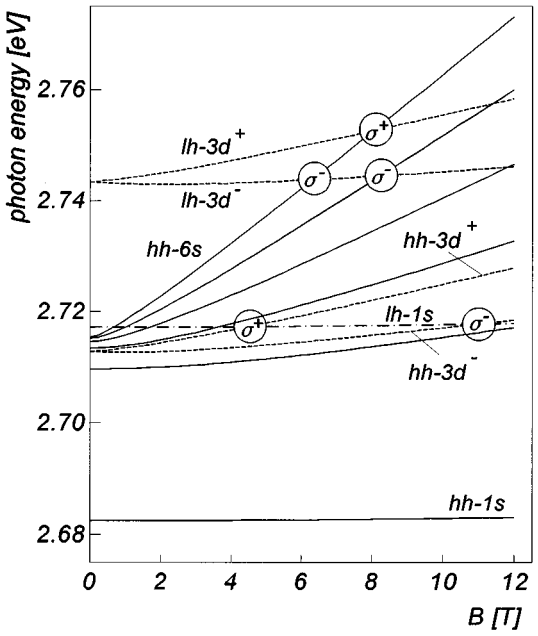

FIG. 5. Computed energies of s-like hh (solid lines), $1s$ lh (dashed-dotted line), and $3d$ hh and lh (dashed lines) magnetoexcitons vs magnetic field. For further explanations see text.

In Fig. 5, the magnetoexciton energies for s-like hh states (solid lines) are given in comparison with those of the lh ground state (dashed-dotted line) as well as hh and lh $3d$ states (dashed lines). Both the hh and lh energies are separately computed within the two-band model by the NSIM method. The data obtained for the $x_{\mathrm{Cd}}=0.13$ sample [Fig. 2(b)] are used. Here, the 1h exciton ground state is placed about 1 meV above E_g^* of the hh band at $B=0$. At the intersections in Fig. 5 marked by a circle containing the respective photon polarization, the hh-lh mixing is resonantly enhanced. For $X_{\mathrm{lh},1s}$ and $X_{\mathrm{hh},3d^-}$, this occurs at fields around 11 T between the $X_{\mathrm{hh},2s}$ and $X_{\mathrm{hh},3s}$ states. Indeed, a respective field-induced absorption feature denoted by $3d^-$ in Fig. 2(b) is found for σ^- polarization at $B\geqslant 10$ T. Both its visibility in a limited range of magnetic fields as well as its low-energy shift with B have to be attributed to the varying coupling strength around the intersection. Due to the larger magnetic field shift of $X_{\mathrm{hh},3d+}$, its mixing with $X_{\mathrm{lh},1s}$ optically active for σ^+ polarization is expected only in a small interval at lower magnetic fields and, thus, not observed here. Recently, both kinds of coupling have been reported for $\mathrm{In}_x\mathrm{Ga}_{1-x}\mathrm{As/GaAs}$ QW's.[32] For the sample with the smallest x_{Cd} in Fig. 3, the lh exciton ground state is placed 2.5 meV below the $X_{\mathrm{hh},2s}$ state. In that case, the valence-band mixing results in a nonmonotonous behavior of $X_{\mathrm{lh},1s}$ clearly seen on the enlarged energy scale. It should be noted that the observed splitting between σ^+ and σ^- polarization is also influenced by the coupling with the $3d^+$ and $3d^-$ hh exciton states, respectively.

According to (11) and (12), the hh exciton ground state can only couple with d-like excited states of the lh exciton. The energetic spacing [nearly given by the sum of the splitting between hh and lh exciton (and the 1h exciton) Rydberg] is so large that this coupling is, however, of minor importance. Practically, the same holds for excited s-like hh exciton states until they are moved into the spectral range of excited 1h states [above 2.74 eV in Fig. 2(b)]. For this reason, the two-band model is quite adequate to describe hh magnetoexcitons with energies below the lh subband gap. Above this energy, clear anticrossing features of the $5s$ and $6s$ hh exciton states are seen at the intersection with $3d$ lh states in Fig. 2(b) (cf. Fig. 5). The spectra in the lower part of Fig. 1 exhibit additional evidence for this. For both magnetic field strengths depicted, the state just located at the crossover, $5s$ or $6s$, has gained an increased oscillator strength.

V. CONCLUSIONS

In conclusion, we have presented a systematic experimental and numerical analysis of magnetoexcitons in wide-gap II-VI-related MQW's. Very precise values of the binding energy as well as the in-plane size and reduced mass of the heavy-hole exciton in $\mathrm{Zn}_x\mathrm{Cd}_{1-x}\mathrm{Se}$ MQW's are gained. The experimental data for the excited exciton states are well reproduced by a numerical solution of the in-plane motion of magnetoexcitons. For the exciton ground state, a variational treatment with a two-parameter trial function yields better agreement. Anticrossing features with different selection rules for σ^+ and σ^- active excitons as well as a nonmonotonous magnetic field behavior of the lh exciton ground state can be well explained by the valence-band mixing. A d-like excited hh exciton state is observed the finite oscillator strength of which results from admixing of the $1s$ lh exciton state.

ACKNOWLEDGMENTS

The authors thank N. Hoffman, J. Griesche, and M. Rabe for the MBE growth. One of us (V.V.R.) is grateful to the Alexander von Humboldt Foundation for the financial support. Part of this work was funded by the Deutsche Forchungsgemeinschaft in the framework of Sfb 296.

*Permanent address: A. F. Ioffe Physico-Technical Institute, St. Petersburg 194 021, Russia.

[1] M. A. Hase, J. Qui, J. M. DePuydt, and H. Cheng, Appl. Phys. Lett. **59**, 2127 (1991); Y. Yamada, Y. Masumoto, J. T. Mullins, and T. Taguchi, *ibid.* **61**, 2190 (1992); A. V. Nurmikko and R. L. Gunshor, Solid State Commun. **92**, 113 (1994).

[2] A. V. Nurmikko and R. L. Gunshor, in *Optics of Semiconductor Nanostructures*, edited by F. Henneberger, St. Schmitt-Rink, and E. Göbel (Akademie Verlag, Berlin, 1993), Chap. II.1; J. Ding, M. Hagerott, P. Kelkar, A. V. Nurmikko, D. C. Grillo, L. He, J. Han, and R. L. Gunshor, Phys. Rev. B **50**, 5787 (1994).

[3] H. J. Lozykowski and V. K. Shastri, J. Appl. Phys. **69**, 3235 (1991).

[4] P. M. Young, E. Runge, M. Ziegler, and H. Ehrenreich, Phys. Rev. B **49**, 7424 (1994).

[5] F. Liagi, P. Bigenwald, O. Briot, B. Gil, N. Briot, T. Cloitre, and R. L. Aulombard, Phys. Rev. B **51**, 4699 (1995).

[6] V. Pellegrini, R. Atanasov, A. Tredicucci, F. Beltram, C. Amzulini, L. Sorba, L. Vanzetti, and A. Franciosi, Phys. Rev. B **51**, 5171 (1995).

[7] R. Cingolani, P. Prete, D. Creco, P. V. Giugno, M. Lomascolo, R. Rinaldi, L. Calcagnile, L. Vanzetti, L. Sorba, and A. Franciosi, Phys. Rev. B **51**, 5176 (1995).
[8] H. Babucke, V. Egorow, P. Thiele, F. Henneberger, M. Rabe, J. Griesche, N. Hoffmann, and K. Jakobs, Phys. Status Solidi B **152**, 161 (1995).
[9] J. C. Maan, G. Belle, A. Fasolino, M. Altarelli, and K. Ploog, Phys. Rev. B **30**, 2253 (1984).
[10] S.-R. E. Yang and L. J. Sham, Phys. Rev. Lett. **58**, 2598 (1987); H. Chu and Y. C. Chang, Phys. Rev. B **40**, 5497 (1989).
[11] N. T. Pelekanos, J. Ding, M. Hagerott, A. V. Nurmikko, H. Luo, N. Sammarth, and J. K. Furdyna, Phys. Rev. B **45**, 6037 (1992).
[12] J. Puls, V. V. Rossin, and F. Henneberger, Mater. Sci. Forum **182-184**, 743 (1995).
[13] J. Engbring and R. Zimmermann, Phys. Status Solidi B **172**, 733 (1992).
[14] G. E. W. Bauer and T. Ando, Phys. Rev. B **38**, 6015 (1988).
[15] The Zeeman spin splitting of electron and hole forming the exciton will not be considered in this section.
[16] D. B. Tran Thoi, R. Zimmermann, M. Grundmann, and D. Bimberg, Phys. Rev. B **42**, 5906 (1990).
[17] H. Haken, *Quantum Field Theory of Solids* (North-Holland, Amsterdam, 1976).
[18] L. P. Gorkov and I. E. Dzyaloshinski, Zh. Éksp. Teor. Fiz. **53**, 717 (1967) [Sov. Phys. JETP **26**, 449 (1968)].
[19] R. Zimmermann, Phys. Status Solidi B **135**, 681 (1986).
[20] J. J. Hopfield and D. G. Thomas, Phys. Rev. **122**, 35 (1961).
[21] O. Akimoto and H. Hasegawa, J. Phys. Soc. Jpn. **22**, 181 (1967).
[22] J. Griesche, N. Hoffmann, and K. Jakobs, J. Cryst. Growth **138**, 59 (1994).
[23] H. E. Gumlich, D. Theis, and D. Tschierse, in *Semiconductors, Physics of Group IV Elements and III-V Compounds* edited by O. Madelung, Landolt-Börnstein, New Series, Group III, Vol. 17, Pt. a (Springer, Berlin, 1987).
[24] B. Sermage and G. Fishman, Phys. Rev. B **23**, 5107 (1981).
[25] H. W. Hölscher, A. Nöthe, and Ch. Uihlein, Phys. Rev. B **31**, 2379 (1985).
[26] To reproduce the experimental E_g^* somewhat smaller values of the Cd content ($\leqslant 2\%$) have to be used in the fit compared to the nominal x_{Cd}.
[27] P. Peyla, R. Romestain, Y. Merle d'Aubigné, G. Fishman, A. Wasiela, and H. Mariette, Phys. Rev. B **52**, 12 026 (1995).
[28] Of course, a variational treatment with a one-parameter trial function [$\gamma=0$ in (5)] results in even less binding energy. Hence, such an ansatz is not very appropriate for the well widths and barrier heights studied here.
[29] Since the effect of the electron spin is purely additive, it does not have to be considered in this context. The spin-orbit hole band is not regarded because it is split off by about 0.4 eV.
[30] By $j_{z,h}$ the hole spin is denoted here, which is just the negative of the valence-band electron spin used in Ref. 14.
[31] M. Potemski, L. Vina, G. E. W. Bauer, J. C. Maan, E. E. Mendez, and W. I. Wang, Phys. Rev. B **43**, 14 707 (1991).
[32] V. D. Kulakovskii, A. Forchel, K. Pieger, J. Straka, B. N. Shepel, and S. V. Nochevny, Phys. Rev. B **50**, 7467 (1994).